

Leidenfrost vapour layer moderation of the drag crisis and trajectories of superhydrophobic and hydrophilic spheres falling in water†

Cite this: *Soft Matter*, 2014, 10, 5662

Ivan U. Vakarelski,^{*a} Derek Y. C. Chan^{bc} and Sigurdur T. Thoroddsen^a

We investigate the dynamic effects of a Leidenfrost vapour layer sustained on the surface of heated steel spheres during free fall in water. We find that a stable vapour layer sustained on the textured superhydrophobic surface of spheres falling through 95 °C water can reduce the hydrodynamic drag by up to 75% and stabilize the sphere trajectory for the Reynolds number between 10^4 and 10^6 , spanning the drag crisis in the absence of the vapour layer. For hydrophilic spheres under the same conditions, the transition to drag reduction and trajectory stability occurs abruptly at a temperature different from the static Leidenfrost point. The observed drag reduction effects are attributed to the disruption of the viscous boundary layer by the vapour layer whose thickness depends on the water temperature. Both the drag reduction and the trajectory stabilization effects are expected to have significant implications for development of sustainable vapour layer based technologies.

Received 16th February 2014
Accepted 9th April 2014

DOI: 10.1039/c4sm00368c

www.rsc.org/softmatter

1 Introduction

The traditional Leidenfrost effect^{1,2} refers to the long lifetime and high lateral mobility of small drops of a liquid that are deposited on a very hot surface. The vapour layer that levitates the drop provides thermal insulation and lubricity and is stable as long as the surface temperature, T_s , is above the Leidenfrost temperature, T_L , that is significantly higher than the boiling point of the liquid. Correspondingly, a hot body at a temperature above T_L that is fully immersed in a liquid will be in the Leidenfrost state, being completely enveloped by a vapour layer that separates it from the liquid, as demonstrated in Fig. 1a for a stationary hot steel sphere in water. When the sphere cools to below T_L , the vapour layer collapses and the resulting solid–liquid contact is manifested as a spectacularly explosive

Leidenfrost transition shown in Fig. 1b.³ Hydrodynamic drag reduction by such an intact gas layer on a textured superhydrophobic surface is a topic of intense current research interest.^{4–7} It is a dynamic analogue of the non-wetting Cassie–Baxter state of water on superhydrophobic surfaces^{8,9} that stimulated recent studies on the combined effects of surface wettability and the Leidenfrost phenomenon.^{3,10–13}

It is well-known that surface modifications such as dimples on the surface of golf balls, the riblet structures on the skin of fast swimming sharks or the addition of small

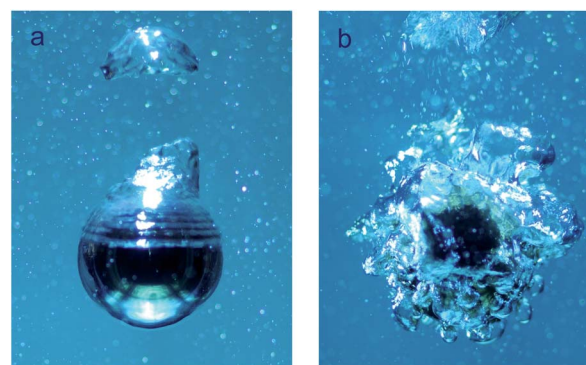


Fig. 1 Snapshots of a stationary 20 mm hydrophilic steel sphere cooling in 95 °C water. (a) The sphere temperature, T_s , is above the Leidenfrost temperature, $T_L = 260$ °C. The Leidenfrost state is characterized by a slow cooling rate as a thin vapour layer streams around the sphere accompanied by vapour bubble pinch off at the upper apex. (b) The explosive Leidenfrost transition as the vapour layer collapses when T_s reaches T_L . Thereafter, the sphere cools rapidly to the pool temperature (see also ref. 3 that contains videos of the process).

^aDivision of Physical Sciences and Engineering and Clean Combustion Research Centre, King Abdullah University of Science and Technology (KAUST), Thuwal 23955-6900, Saudi Arabia. E-mail: ivanuriev.vakarelski@kaust.edu.sa

^bDepartment of Mathematics and Statistics, The University of Melbourne, Parkville 3010, Australia

^cDepartment of Chemistry and Biotechnology, Swinburne University of Technology, Hawthorn 3122, Australia

† Electronic supplementary information (ESI) available: A pdf file containing Fig. S1–S4. Fig. S1: photograph of the water vessel and heater device; Fig. S2: heat transfer coefficient vs. sphere temperature dependence; Fig. S3: examples for the fall distance vs. time data; Fig. S4: collection of velocity vs. time data for 15 mm (a); 20 mm (b); 30 mm (c); 40 mm (e) spheres. Video 1: this combined video parallels the fall of a 20 cm steel sphere in 95 °C water: the left side is for a 95 °C hydrophilic sphere and the right side is for a 200 °C superhydrophobic sphere. The video is shot at the lower part of the tank where the spheres approach the terminal velocity. The frame rate used was 1000 fps and the video playback speed was 30 fps. See DOI: 10.1039/c4sm00368c

amounts of soluble polymers in water can reduce the hydrodynamic drag on moving bodies.^{14–17} But despite potential benefits in energy efficient transport ranging from ocean liners to microfluidics, previous attempts to quantify drag reduction of spheres in water using surface gas layers produced only a moderate effect.^{18–22} Previously, we have shown that a continuous Leidenfrost vapour layer on a heated steel sphere in a simple fluorocarbon liquid (FC-72 comprising mainly perfluorohexane C₆F₁₄) can reduce the hydrodynamic drag on a falling sphere by up to 85%.²³ However, producing the same effect in water is far more challenging because it is very difficult to sustain a stable Leidenfrost vapour layer in water due to the higher vaporization heat capacity of water (30 times higher than FC-72) combined with a higher boiling temperature (56 °C for FC-72 vs. 100 °C for water) and a higher surface tension (12 mN m⁻¹ for FC-72 vs. 72 mN m⁻¹ for water). A further challenge highlighted in the present work is that the Leidenfrost temperature for a sphere falling through water is significantly higher than the Leidenfrost temperature for a static sphere.

In this paper we present results of a systematic investigation of the vapour layer induced drag reduction on spheres falling in water. Recent sphere-cooling experiments in water³ and sessile drop experiments on a heated substrate^{10–12} have demonstrated that the sustainability of the vapour layer depends strongly on the wetting properties of the solid surface. In fact, the cooling of an overheated superhydrophobic steel sphere in water can take place entirely in the continuous vapour layer or the Leidenfrost regime, without transition to the nucleate boiling regime and the accompanied vapour explosion that is always observed in the case of non-superhydrophobic surfaces.³ Therefore we seek to enhance the stability of the vapour layers by using textured superhydrophobic surfaces and conduct the experiments in water heated up to 95 °C as the thickness of such stable vapour layers also varies with the water temperature.

2 Experimental

In the present experiments we use high-speed video recording to measure the velocity of steel spheres with diameters, $d = 2R$, ranging from 10 mm to 40 mm falling through water held in a tank of height 2 m and cross-sectional dimensions 20 × 20 cm (ESI Fig. S1†). Two types of sphere surfaces were used: the smooth polished hydrophilic surface (water contact angle < 30°) and the textured superhydrophobic surface (water contact angle > 160°).

2.1 Steel sphere modification

The spheres used were polished stainless steel grinding balls (FRITSCH GmbH) of density $\rho_s = 7700 \text{ kg m}^{-3}$ and diameters $d = 10, 15, 20, 25, 30$ and 40 mm. The average surface roughness given by the manufacturer is $R_a < 0.06 \text{ }\mu\text{m}$. Using an electrical discharge machine, we drilled a 0.5 mm diameter hole radially to the center of each sphere. A small metallic wire hook was

fitted in the hole to facilitate handling of the sphere without having to touch the sphere surface. The wire hook was also used to hang the sphere inside the heating furnace and to carry the heated sphere using metallic forceps. A thermal couple could also be inserted into the hole to measure the sphere temperature.

Spheres with a hydrophilic surface were prepared from the unmodified steel spheres after thorough washing with acetone, ethanol and water resulting in water contact angles of less than 10°. After heating the spheres to a temperature of about 500 °C the spheres remained hydrophilic with an average water contact angle of not more than 30°.

Spheres with superhydrophobic surfaces were made by applying a coating of a commercially available car mirror water-repellent agent (Glaco Mirror Coat “Zero”, Soft 99 Co.). The liquid coating is an alcohol-based suspension of silica nanoparticles functionalized by an organic hydrophobizing agent. A detailed description of the coating deposition procedure and characterization of the superhydrophobic coating properties is given in ref. 3. In brief, the clean sphere was washed with the coating suspension liquid and then heat cured at about 300 °C for 30 minutes. Repeating the agent wash and heat cure process a further two times gave excellent superhydrophobic surface properties with a water contact angle of more than 160°. The coating has two scales of roughness: a coarse scale with 0.5–2.0 μm structures of nanoparticle aggregates and a smaller nano-scale roughness that is characteristic of the size of the nanoparticles of about 50 nm.³

2.2 Free falling sphere experiments

The water tank and heater device used to conduct the falling sphere experiments was custom manufactured by ChangTong Science and Technology (TianJin) Co. LTD, China. A photograph of the device is given in ESI Fig. S1.† The water tank is 2 m tall and has a cross-sectional area of 20 × 20 cm. The front and back walls of the tank are double-glazed fortified glass windows. The two side walls of the tank are also double-walled for improved thermal insulation. Electric heaters are installed in a heater chamber beneath the tank base that can heat the water in the tank up to the boiling temperature of 100 °C. Thermocouple probes were used to monitor the water temperature inside the tank. After heating the water to the desired temperature the electric heaters were switched-off during the falling sphere experiments to suppress water thermal convections and for safety considerations. Several minutes after the heaters were switched-off, the temperature of the water in the tank was found to be uniform to within $\pm 1 \text{ }^\circ\text{C}$ from the bottom to about 2 cm below the water surface at the top. The working temperature for the experiments was maintained to be within $\pm 1 \text{ }^\circ\text{C}$ as measured at a control point about 20 cm below the water surface.

Spheres were heated to the desired temperature in a temperature control furnace for at least 30 minutes. The heated spheres were held by metal forceps and carefully released from below the water surface at the top of the tank. The sphere fall was monitored using a high-speed video camera (Photron

Fastcam SA-3) with a typical filming frame rate of 1000 fps. The sphere trajectory coordinates *vs.* time and the corresponding instantaneous velocity were determined by image processing the videos with the camera software (Photron FASTCAM Viewer, PFV Ver.3262). An example for the fall distance *vs.* time data obtained by processing the sphere fall videos is given in ESI Fig. S3.†

2.3 Determination of the drag coefficients

The hydrodynamic drag on a sphere moving at velocity U is characterized in terms of the variation of the standard drag coefficient defined by $C_D = 2F_D/(\pi R^2 \rho U^2)$ with the Reynolds number $Re = 2\rho R U/\mu$. Here F_D is the drag force on the sphere, ρ the fluid density, R the sphere radius and μ the dynamic shear viscosity of the fluid. In free falling sphere experiments, the drag coefficient is determined from the sphere terminal velocity, U_T , using the relationship:

$$C_D = (8[\rho_s - \rho]gR)/(3\rho U_T^2) \quad (1)$$

where g is the gravitational acceleration and ρ_s the sphere density. The terminal velocity was corrected for the effect of the tank walls using the following correction formula according to Newton (1687):

$$U_T/U_{T\infty} = [1 - (d/D)^2][1 - 0.5(d/D)^2]^{1/2} \quad (2)$$

where U_T is the measured terminal velocity, $U_{T\infty}$ is the corrected terminal velocity for the infinite flow domain, $d = 2R$ is the sphere diameter and D is the diameter of a cylindrical tank. For the $a \times a$ square cross-section tank used in the present experiment, the effective diameter D in eqn (2) is calculated by equating the areas of the circle and the square, *i.e.* $D = (2/\sqrt{\pi})a$.²⁴

2.4 Sphere cooling rates

The temperature of the sphere that was held stationary under water was monitored by a thermocouple probe inserted into the sphere center. Further details for these measurements can be found in ref. 3 that also contains videos of the cooling process in each case. The time dependence of the temperature of a 20 mm steel sphere cooling in 24 °C, 85 °C and in 95 °C water is shown in Fig. 2a for a hydrophilic sphere, and in Fig. 2b for a superhydrophobic sphere. For the hydrophilic sphere the results show an abrupt transition from the Leidenfrost regime to the nucleate boiling regime at the Leidenfrost temperature T_L of about 440 °C in 24 °C water, T_L of about 280 °C in 85 °C water and T_L of about 260 °C in 95 °C water (Fig. S4a†). This transition at the Leidenfrost point (LP in Fig. 2a) is characterized by an explosive transition to the nucleate boiling regime (see Fig. 1b). As could be expected for the hydrophilic spheres the Leidenfrost temperature decreases with increasing pool temperature.²⁵ In the case of a superhydrophobic sphere, the cooling is entirely in the Leidenfrost regime without transition to the nucleate boiling regime³ (Fig. 2b).

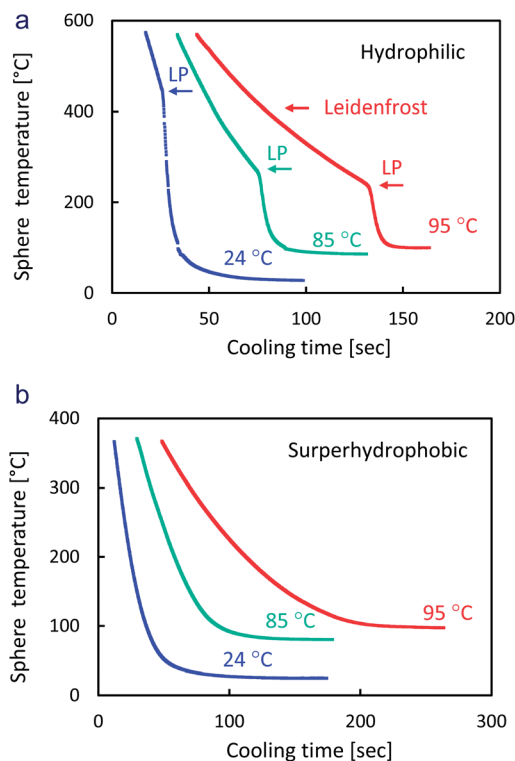


Fig. 2 Sphere temperature *vs.* cooling time for a statically held 20 mm steel sphere cooled in 24 °C water (blue line), 85 °C (green line) or 95 °C water (red line): (a) hydrophilic sphere and (b) superhydrophobic sphere. Arrows on (a) mark the Leidenfrost point (LP) characterized by an explosive transition to the nucleate boiling regime.³ ESI Fig. S2† shows data for the corresponding heat transfer coefficients.

3 Results and discussion

3.1 Trials in room temperature 95 °C and 85 °C water

In the initial trials we measured the velocity of heated steel spheres falling in water at 24 °C (room temperature). Fig. 3 shows data for the terminal velocity dependence on the sphere temperature in the case of 40 mm hydrophilic and superhydrophobic steel spheres ($Re \sim 1.0 \times 10^5$ to 1.5×10^5). For the 40 mm hydrophilic sphere with the initial sphere temperature between 300 °C and 700 °C we observed about a 35% increase in the terminal velocity compared to the room temperature sphere (Fig. 3). However, the vapour layer around the falling hydrophilic sphere always collapsed shortly after the sphere release even for spheres heated to 800 °C, well above the static sphere Leidenfrost temperature of about 440 °C (Fig. 2a). The collapse or destabilization of the Leidenfrost layer was confirmed visually as shortly after the sphere release, we observe a bubble cloud burst from the sphere surface. It can be assumed that the vapour layer destabilization is initiated by the shear stresses induced on the layer during the sphere fall. All the data points shown in Fig. 3 for the hydrophilic sphere should thus be regarded as results corresponding to the absence of a vapour layer. The drag reduction effect in that case is due to the combined effects of heating up the water around the falling sphere resulting in a reduction of viscosity in the boundary layer

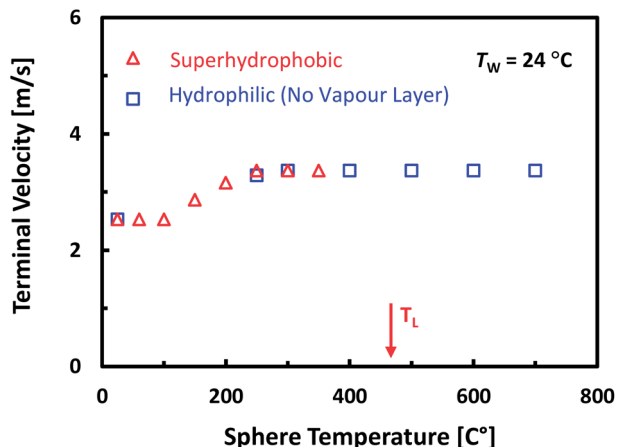


Fig. 3 Variation of the terminal velocity with the sphere temperature measured for a 40 mm steel sphere falling through room temperature (24 °C) water. Open square data points (blue) are for the hydrophilic sphere and open triangles data (red) are for the superhydrophobic sphere. Notice that although a static hydrophilic sphere will be in the Leidenfrost regime for $T_s > 440$ °C, the vapour layer is destroyed shortly after the sphere release to free fall even for spheres with the initial T_s as high as 700 °C. All hydrophilic sphere data points thus represent the vapour layer free case.

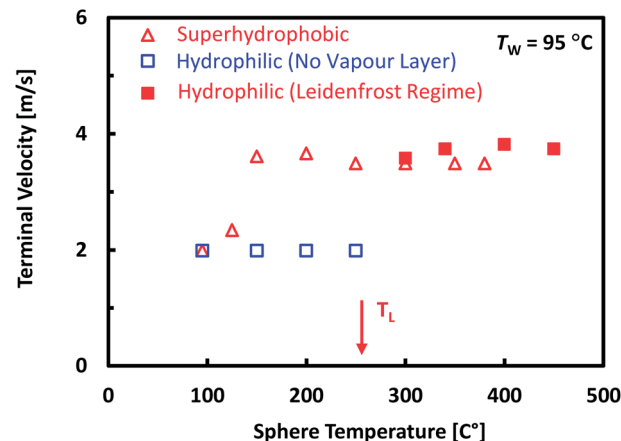


Fig. 4 Variation of the terminal velocity with the sphere temperature, measured for a 20 mm steel sphere falling through 95 °C water. Open squares (blue) are data for hydrophilic spheres at temperatures below the Leidenfrost temperature ($T_L = 260$ °C) and solid squares (red) for temperatures above T_L . Open triangles (red) are data for superhydrophobic spheres (see also Video 1†).

and the shedding of small bubbles from the sphere surface that correspond to the regime of nucleate boiling. The relative contributions of these effects are not easy to quantify.

For 40 mm superhydrophobic spheres we measured a similar increase of about 35% in the terminal velocity with the increase of the sphere temperature to about 300 °C (Fig. 3). For the superhydrophobic sphere, the Leidenfrost vapour layer remained intact as we did not observe any destabilization or collapse of the vapour layer as the sphere fell. This is in contrast to the case of the hydrophilic sphere, and one can assume that the drag reduction was due predominantly to the presence of the Leidenfrost regime vapour layer. However considering that the vapour free heated hydrophilic sphere shows a similar drag reduction it remains unclear whether the drag reduction effect for the superhydrophobic sphere in 24 °C water is primarily due to the vapour layer around the sphere or due to the heating of the water in the vicinity of the sphere.

In order to resolve the ambiguity in the interpretation of the data in room temperature water we chose to conduct experiments in water heated up to 95 °C. In water heated to near the boiling point, a stable vapour layer can be easily sustained on the falling sphere and at the same time the effect of the water heating on the spheres is negligible. An added advantage is that the viscosity of water at 95 °C is about three times lower than the water viscosity at room temperature and this helps to extend the experimental Reynolds numbers to beyond the critical value.

In Fig. 4 we quantify the effects of surface treatment on the vapour layer by comparing the temperature variation of the terminal velocity of 20 mm diameter hydrophilic and superhydrophobic steel spheres falling in 95 °C water. For the

hydrophilic sphere it was possible to sustain a stable vapour layer on the falling sphere for temperatures $T_s > 300$ °C that is only slightly higher than the static sphere Leidenfrost temperature of about 260 °C (Fig. 2b). This transition to the Leidenfrost regime is observed as a sharp increase of the terminal velocity of the sphere from about 1.9 m s⁻¹ to about 3.8 m s⁻¹ corresponding to a decrease of the drag force on the sphere by about 75%. The dramatic speed difference is illustrated in ESI Video 1.† The drag reduction observed under these conditions is of the same magnitude as that observed for Leidenfrost spheres falling in a fluorinated liquid.²³ The results for the superhydrophobic sphere demonstrate that the additional textured superhydrophobic surface property enhances the Leidenfrost vapour layer stability under dynamic conditions so that the drag reduction effect is observable even at a lower sphere temperature of 125 °C (25 °C overheat) and is fully developed above 150 °C (50 °C overheat).

In Fig. 5, we present results for 20 mm spheres falling in water heated to about 85 °C which show transient behaviour between that for room temperature water and 95 °C water. In 85 °C water, the moving hydrophilic sphere does transition to a Leidenfrost regime but at a temperature above 500 °C which is substantially higher than the static sphere Leidenfrost temperature, $T_L \sim 280$ °C (Fig. 2a). In contrast, drag reduction for the superhydrophobic spheres is already noticeable at a temperature of about 150 °C but becomes fully developed only at temperatures above 300 °C.

3.2 Reynolds number dependence

Next we elucidate the dependence of drag reduction on the Reynolds number by conducting an experiment with steel spheres of different sizes falling in 95 °C water. The experimental range of Reynolds numbers covered in these measurements: $10^4 < Re < 10^6$ (water at 95 °C, $\rho = 0.96$ kg m⁻³,

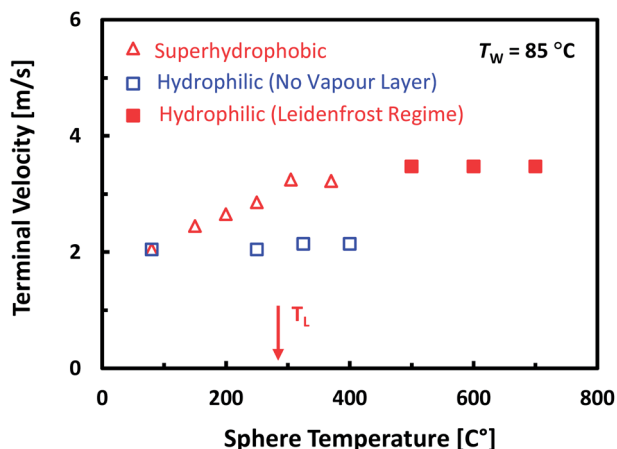


Fig. 5 Variation of the terminal velocity with the sphere temperature, measured for a 20 mm steel sphere falling through 85 °C water. Data showing the gradual development of drag reduction for superhydrophobic spheres are shown as open (red) triangles. Data for hydrophilic spheres show no drag reduction below 500 °C (open blue squares) and the sudden development of full drag reduction (solid red squares) above 500 °C for spheres falling in the Leidenfrost regime. The static Leidenfrost temperature $T_L \sim 280$ °C of the hydrophilic sphere in 85 °C water is indicated.

$\mu = 0.03$ mPa s) spans the location of the drag crisis for a free falling solid sphere at which the drag coefficient C_D drops rapidly from 0.5 to 0.2 at $Re \sim 3 \times 10^5$.

In Fig. 6 we compare the drag coefficients for hydrophilic spheres at temperature $T_S = 95$ °C, the same temperature as the water where there is no vapour layer, with the drag coefficient of

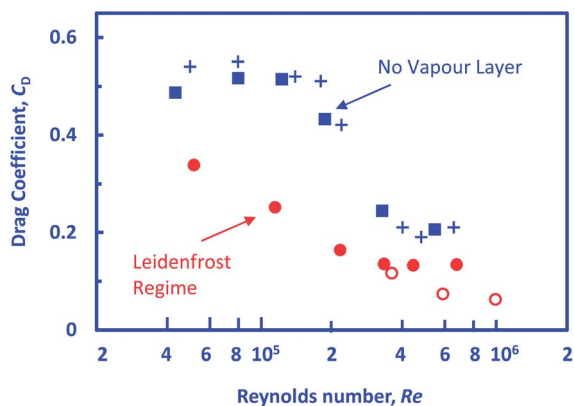


Fig. 6 Dependence of the drag coefficient on the Reynolds number for steel spheres ($2R = 10; 15; 20; 25; 30; 40$ mm) falling in 95 °C water. Solid squares (blue) are for hydrophilic spheres at a sphere temperature $T_S = 95$ °C, where no vapour layer is present, and solid circles (red) are for superhydrophobic spheres at a sphere temperature $T_S = 200$ °C in the Leidenfrost regime. Both sets of results are calculated using the sphere velocity at the end of the 2 m fall. Open circles (red) are for 200 °C superhydrophobic spheres calculated using the extrapolated values for the terminal velocity (ESI Fig. S4†). Literature values for smooth solid spheres falling in an "infinite" tank measured by White¹⁵ are shown as blue crosses.

superhydrophobic spheres at $T_S = 200$ °C, at which a stable Leidenfrost vapour layer surrounds the sphere. The results for hydrophilic spheres (no vapour layer) follow closely literature data for solid spheres falling in water that exhibit the characteristic onset of the drag crises at the critical $Re \sim 3 \times 10^5$. This is associated with the rapid decrease of the drag coefficient from the sub-crisis value of about 0.5 through the minimum value of about 0.2.^{15,16} In contrast, superhydrophobic spheres in the Leidenfrost regime ($T_S = 200$ °C) with a surface vapour layer exhibit a gradual decrease in the drag coefficient for $Re > 10^4$ that follows the same trend demonstrated before for a fluorinated liquid.²³

For spheres released from rest, the time dependence of the velocity, $U(t)$, is observed to evolve towards the terminal value, U_T , according to the exponential form:¹⁶

$$U(t) = U_T(1 - e^{-t/\tau}) \quad (3)$$

As discussed in ref. 16 this equation does not accurately present the complex dynamics of the true fall trajectory, but could be used as an effective tool to estimate the terminal velocity. Results for the drag coefficient shown in Fig. 6, shown as solid squares for the no-vapour hydrophilic case and solid circles for the Leidenfrost regime, are calculated using the sphere velocity measured close to the bottom of the 2 m water tank. However, for a higher Reynolds number ($Re > 2 \times 10^5$), the velocity after the 2 m fall has not yet reached the terminal value as detailed in ESI Fig. S4† data. In such cases, eqn (3) can be used to estimate the terminal velocity that is then used to calculate the corresponding drag coefficient and Reynolds number represented as open circles in Fig. 6. These extrapolated results indicate the gradually decreasing trend of the drag force with increasing Re in the Leidenfrost regime is valid up to the maximum investigated limit of $Re \sim 10^6$ exceeding the location of the drag crises minimum in the no vapour layer case.

3.3 Stabilisation of the fall trajectory

We found that the Leidenfrost vapour layer not only reduces the drag but also has a dramatic effect on the stability of the trajectory of the falling sphere. This is demonstrated in Fig. 7 for the case of 40 mm spheres falling in 95 °C water. In the absence of the Leidenfrost vapour layer (Fig. 7a) the sphere trajectories exhibit large, random deviations from rectilinear motion that are due to non-axisymmetric, flow structures contained in the sphere wake^{26,27} that perturb the sphere trajectory. In contrast in the Leidenfrost regime the sphere fall trajectory is almost perfectly linear (Fig. 7b) and this is in accordance with a smaller and more symmetrical wake observed behind spheres falling in the Leidenfrost regime.²³ This is the first time we report this phenomenon that may prompt further investigations with important practical implications for the vapour layers drag reduction related applications. However, indications of this effect were evident in our earlier studies conducted in fluorinated liquids²³ even though they were not reported.

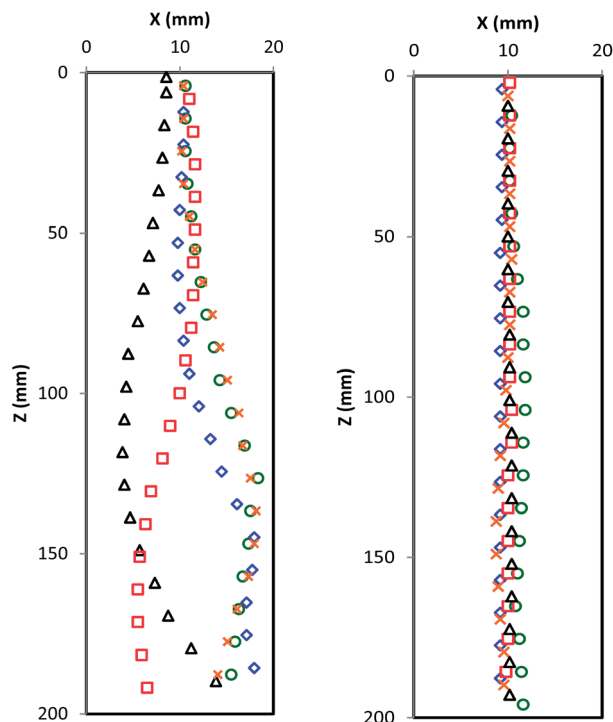


Fig. 7 Examples of the trajectories of 40 mm steel spheres falling in 95 °C water: (a) $T_s = 95$ °C hydrophilic spheres with no vapour layer and (b) $T_s = 200$ °C superhydrophobic spheres in the Leidenfrost regime in the presence of a vapour layer. The horizontal and vertical (X , Z) trajectory coordinates are obtained from high speed video recording of five independent runs with each trajectory represented by a different symbol.

3.4 Correlation with the vapour layer thickness

For the range of the Reynolds number investigated here ($Re \sim 10^4$ to 10^6) the predominant component of the drag force on the sphere is due to the pressure-induced form or wake drag with the viscous or skin friction drag accounting for less than 5% of the total drag on the sphere.²⁸ In our earlier study,²³ we demonstrated the correlation between the reduction in the drag coefficient and the relocation of the separation point of the boundary layer towards the rear of the sphere in the Leidenfrost regime. It is well known that the drag crisis in the no-vapour layer case is associated with the moving of the flow separation point to the rear of the sphere when the transition to the turbulent boundary layer occurs. Although the presence of the Leidenfrost vapour layer also moves the separation point, the underlying physical mechanism is due to changing the no-slip boundary condition for the solid-liquid boundary layer with the one that might be closer to the stress-free boundary condition for the vapour-liquid boundary layer.^{29,30}

McHale *et al.*²² have reported correlations between the drag reduction on superhydrophobic surfaces of various textures and the thickness of the surface sustained air layer or plastron. However, in our experiment we found no change in the drag on the unheated superhydrophobic sphere falling in room temperature water (Fig. 3). This indicates that the naturally

sustained air layer on the type of superhydrophobic surface used here is not thick enough to provide measurable drag reduction effects. We can further quantify the vapour layer thickness effect by comparing the thickness of the Leidenfrost vapour layer to that of the viscous boundary layer. The thickness of the Leidenfrost vapour layer, δ_L , can be estimated from the cooling rate in the Leidenfrost regime using the following relationship:³¹

$$\delta_L = \left(\frac{3k_v}{\rho_s c_p R} \right) \frac{(T_s - T_{sat})}{(dT/dt)} \quad (4)$$

where $\rho_s = 7700$ kg m⁻³ is the sphere density, $c_p = 466$ J kg⁻¹ K⁻¹ is the sphere specific heat, (dT/dt) is the sphere cooling rate, $k_v = 0.016$ W m⁻¹ s⁻¹ is the water vapour thermal conductivity and $T_{sat} = 100$ °C is the saturation temperature. Fig. 8 shows the vapour film thicknesses estimated using the static superhydrophobic sphere cooling rate data (Fig. 2b). As the sphere temperature T_s varies between 150 °C and 350 °C, we find $\delta_L \sim 50$ –110 μ m in 95 °C water. The vapour layer thickness estimated from cooling rate data taken at 85 °C water is about 2.5 times thinner than that at 95 °C and this may account for the quantitative variation in drag reduction at different water temperatures. However, in both cases, the vapour layer thickness is comparable to the typical estimate for the viscous boundary layer thickness:²⁹

$$\delta_B \sim (2\mu R/\rho U_T)^{1/2} \sim 50 \mu\text{m} \quad (5)$$

This would suggest that the Leidenfrost vapour layer acts as a surface feature with a variable characteristic length that is responsible for the gradual reduction in the drag coefficient rather than an abrupt drag crisis transition for a surface with fixed geometric features. A similar gradual reduction in the drag coefficient has also been reported when a low (5 ppm) concentration of polymer has been added to the water where polymer coil-stretching in the boundary layer is attributed as the drag reduction mechanism.¹⁶

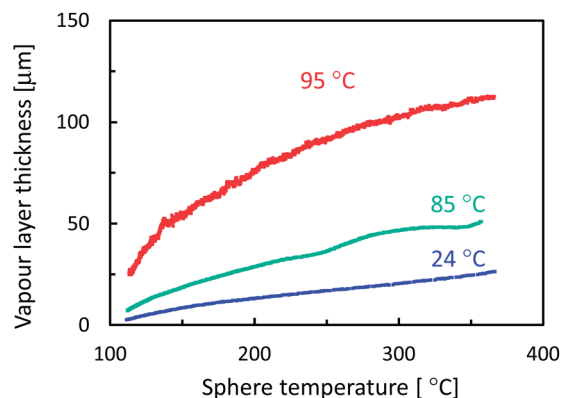


Fig. 8 Vapour layer thickness vs. sphere temperature for a 20 mm superhydrophobic steel sphere cooling in 24 °C water (blue line), 85 °C (green line) and 95 °C water (red line), calculated using Fig. 2b data and eqn (4).

4 Conclusions

This study has elucidated conditions under which large and sustained drag reduction and trajectory stabilization for hot steel spheres falling in water can be achieved using stable continuous vapour surface layers. Due to the high heat transfer coefficient of water compared to simple liquids, it is known to be difficult to sustain a stable vapour layer on moving surfaces. For hot spheres with a superhydrophobic surface, a stable vapour layer can always be maintained at the surface and full drag reduction is attained at a sphere temperature of ~ 150 °C in 95 °C water and ~ 300 °C in 85 °C water. We attribute this dependence on the water temperature to the variations of the thickness of the stable vapour layer. The threshold thickness of the vapour layer for the development of the drag reduction is correlated with the thickness of the viscous boundary layer. For hot spheres with a hydrophilic surface, the transition to full drag reduction is sudden and occurs close to the static Leidenfrost temperature of $T_L \sim 260$ °C in 95 °C water. However, in 85 °C water, the transition occurs at ~ 500 °C, well above the static Leidenfrost temperature of $T_L \sim 280$ °C. Thus the critical transition temperature to drag reduction for a hydrophilic sphere differs from the familiar static Leidenfrost temperature. Finally, the drag reduction and the associated stabilization of the fall trajectory operate at Reynolds numbers exceeding the drag crisis minimum observed in the absence of vapour layers. These results will hopefully help stimulate current effort to develop inexpensive drag reduction technologies based on the sustainability of the air layer on the textured superhydrophobic surface.

Acknowledgements

We acknowledge G. D. Li from the KAUST Solar and Photovoltaics Research Center for assisting in the water tank and heater device design, and the KAUST Machine Workshop for the support in setting the experiments. This work is supported in part by an Australian Research Council Discovery Project Grant to DYCC.

Notes and references

- 1 J. G. Leidenfrost, *De Aquae Communis Nonnullis Qualitatibus Tractatus*, 1756; J. G. Leidenfrost, *Int. J. Heat Mass Transfer*, 1966, **9**, 1153.
- 2 D. Quéré, *Annu. Rev. Fluid Mech.*, 2013, **45**, 197.
- 3 I. U. Vakarelski, N. A. Patankar, J. O. Marston, D. Y. C. Chan and S. T. Thoroddsen, *Nature*, 2012, **489**, 274.
- 4 J. P. Rothstein, *Annu. Rev. Fluid Mech.*, 2010, **42**, 89.
- 5 G. McHale, M. I. Newton and N. J. Shirtcliffe, *Soft Matter*, 2010, **6**, 714.
- 6 H. Dong, M. Cheng, Y. Zhang, H. Wei and F. Shi, *J. Mater. Chem. A*, 2013, **1**, 5886.
- 7 B. Wang, J. Wang, Z. Dou and D. Chen, *Ocean Eng.*, 2014, **79**, 58.
- 8 A. B. D. Cassie and S. Baxter, *Trans. Faraday Soc.*, 1944, **40**, 0546.
- 9 D. Quere, *Annu. Rev. Mater. Res.*, 2008, **38**, 71.
- 10 G. Liu, L. Fu, A. V. Rode and V. S. J. Craig, *Langmuir*, 2011, **27**, 2595.
- 11 H. Kim, B. Truong, J. Buongiorno and L. Hu, *Appl. Phys. Lett.*, 2011, **98**, 083121.
- 12 D. A. del Cerro, A. G. Marín, G. R. B. E. Romer, B. Pathiraj, D. Lohse and A. J. H. Veld, *Langmuir*, 2012, **28**, 15106.
- 13 I. U. Vakarelski, D. Y. C. Chan, J. O. Marston and S. T. Thoroddsen, *Langmuir*, 2013, **29**, 11074.
- 14 P. W. Bearman and J. K. Harvey, *Aeronaut. Q.*, 1976, **27**, 112.
- 15 A. White, *Nature*, 1965, **216**, 994.
- 16 N. Lyotard, W. L. Shew, L. Bocquet and J.-F. Pinton, *Eur. Phys. J. B*, 2007, **60**, 469.
- 17 B. Dean and B. Bhushan, *Philos. Trans. R. Soc., A*, 2010, **368**, 4775.
- 18 W. S. Bradfield, R. O. Barkdoll and J. T. Byrne, *Int. J. Heat Mass Transfer*, 1962, **5**, 615.
- 19 Y. Zvirin, G. R. Hewitt and D. B. R. Kenning, *Exp. Heat Transfer*, 1990, **3**, 185.
- 20 F. S. Gunnerson and P. R. Chappidi, in *Dynamic Aspects of Explosion Phenomena*, AIAA, New York, 1993, pp. 322–333.
- 21 L. Meyer, *Nucl. Eng. Des.*, 1999, **189**, 191.
- 22 G. McHale, N. J. Shirtcliffe, C. R. Evans and M. I. Newton, *Appl. Phys. Lett.*, 2009, **94**, 064104.
- 23 I. U. Vakarelski, J. O. Marston, D. Y. C. Chan and S. T. Thoroddsen, *Phys. Rev. Lett.*, 2011, **106**, 214501.
- 24 R. P. Chhabra, P. H. T. Uhlherr and J. F. Richardson, *Chem. Eng. Sci.*, 1996, **51**, 4531.
- 25 V. K. Dhir and G. P. Purohit, *Nucl. Eng. Des.*, 1978, **47**, 49.
- 26 S. Taneda, *J. Fluid Mech.*, 1978, **85**, 187.
- 27 M. Horowitz and C. H. K. Williamson, *J. Fluid Mech.*, 2010, **651**, 251.
- 28 E. Achenbach, *J. Fluid Mech.*, 1972, **54**, 565.
- 29 H. Schlichting, *Boundary Layer Theory*, McGraw-Hill Book Company, 1979.
- 30 D. W. Moore, *J. Fluid Mech.*, 1965, **23**, 749.
- 31 H. Jouhara and B. P. Axcell, *Nucl. Eng. Des.*, 2009, **239**, 1885.